REPORT
212

PROVENANCE FINGERPRINTING OF GOLD FROM THE KURNALPI GOLDFIELD

by
EA Hancock and TJ Beardsmore

Government of **Western Australia**
Department of **Mines, Industry Regulation and Safety**

Geological Survey of Western Australia

Government of **Western Australia**
Department of **Mines, Industry Regulation and Safety**

REPORT 212

PROVENANCE FINGERPRINTING OF GOLD FROM THE KURNALPI GOLDFIELD

by
EA Hancock and TJ Beardsmore

PERTH 2020

Geological Survey of Western Australia

MINISTER FOR MINES AND PETROLEUM
Hon Bill Johnston MLA

DIRECTOR GENERAL, DEPARTMENT OF MINES, INDUSTRY REGULATION AND SAFETY
David Smith

EXECUTIVE DIRECTOR, GEOLOGICAL SURVEY AND RESOURCE STRATEGY
Jeff Haworth

REFERENCE
The recommended reference for this publication is:
Hancock, EA and Beardsmore, TJ 2020, Provenance fingerprinting of gold from the Kurnalpi Goldfield: Geological Survey of Western Australia, Report 212, 21p.

ISBN 978-1-74168-916-7
ISSN 1834-2280

A catalogue record for this book is available from the National Library of Australia

Grid references in this publication refer to the Geocentric Datum of Australia 1994 (GDA94). Locations mentioned in the text are referenced using Map Grid Australia (MGA) coordinates, Zone 50. All locations are quoted to at least the nearest 100 m.

Published 2020 by the Geological Survey of Western Australia
This Report is published in digital format (PDF) and is available online at <www.dmirs.wa.gov.au/GSWApublications>.

Further details of geoscience publications are available from:
Information Centre
Department of Mines, Industry Regulation and Safety
100 Plain Street
EAST PERTH WESTERN AUSTRALIA 6004
Telephone: +61 8 9222 3459 Email: publications@dmirs.wa.gov.au
www.dmirs.wa.gov.au/GSWApublications

Cover image: Gold nuggets extracted from regolith in Discovery Hill, Kurnalpi Terrain. They are slightly rounded, intergrown with milky quartz and have an angular, irregular shape with a pitted spongy surface

Contents

Figures

Tables

Appendices

Available with the PDF online as an accompanying digital resource

Provenance fingerprinting of gold from the Kurnalpi Goldfield

by

EA Hancock and TJ Beardsmore

Abstract

For a study of the provenance, metallogenesis and prospectivity of placer gold in the Kurnalpi Terrane, KalNorth Gold Mines Limited provided the Geological Survey of Western Australia (GSWA) a suite of 274 (389.9 g) gold nuggets from 37 sites over an area of about 80 km^2 distributed across the Kurnalpi goldfield in Western Australia. GSWA selected 75 (169.4 g) representative gold nuggets for analyses of grain microstructure, silver and trace-element chemistry, inclusion and gangue mineralogy. The data constrain the proximity of nuggets to their primary source(s), the composition of the mineralizing fluids, the primary mineral deposit type(s), and post-mineralization events. Our study shows that all nuggets have a hypogene origin, based on their relatively high Ag content from 3 to 12 wt%, micro-inclusions of Ag/Au/Bi-tellurides, galena, arsenopyrite, and pyrite, and their crystalline microstructure. Only Cu and Hg are consistently present as trace elements in gold grains, with mean concentrations of 100–200 ppm and 50–100 ppm, respectively. Traces of Sb, Te, Pb, and Bi are present only locally. The original microstructure of gold nuggets is mostly preserved and just partly impacted by the supergene processes. There is only local recrystallization around inclusions of regolith materials and along thin marginal rims that formed from supergene weathering and mechanical mobilization of the nuggets. We conclude that most gold nuggets were collected proximal to their primary sources and were altered in situ during their relatively prolonged residence in the regolith. Variations in gold morphology and regolith inclusions result from local supergene environment conditions during gold deposition and its residence. Primary mineralization appears to be quartz vein hosted with two types of mineral assemblages: gold–arsenopyrite–pyrite and gold–galena–chalcopyrite with Te-bearing minerals.

KEYWORDS: crystal structure, fingerprinting, gold minerals, gold placer deposits, LA-ICPMS, trace elements, scanning electron microscopy

Introduction

Placer gold nuggets are commonly liberated fragments from primary hypogene mineralization (e.g. Liversidge, 1893; Petrovskaya, 1973; Wilson, 1984; Hough et al., 2007; Butt and Timms, 2011). Their morphology, microstructure, chemistry, and accessory inclusions can provide important information about the composition of the mineralizing hydrothermal fluid, physical and chemical depositional conditions, proximity to the primary source, primary mineral deposit type, and post-mineralization modification processes (e.g. Chapman et al., 2002; Hancock et al., 2009; Hancock and Thorne, 2011; Nikiforova et al., 2011, 2013; Nikolaeva et al., 2004, 2013; Tetland, 2015).

Characteristics of placer gold nuggets potentially provide information about the nature and proximity of the primary bedrock gold systems from which they were derived. These relationships can be used as vectors for the discovery of bedrock gold deposits.

To test this premise, the Geological Survey of Western Australia (GSWA) has undertaken a pilot study of 274 gold nuggets from 37 sites distributed across the Kurnalpi goldfield in Western Australia (Fig. 1). This pilot study aims to develop analytical techniques and demonstrate the efficacy of the research approach, with the ultimate goal of expanding the research scope to include a systematic appraisal of gold-mineralized provinces throughout Western Australia.

The Kurnalpi study area was chosen due to the availability of gold nuggets through the support of KalNorth Gold Mines Limited (KGM). The samples are widely distributed in the area of about 80 km^2 and were systematically collected and accurately georeferenced. This study involved two discrete, but interrelated components:

Regolith and landscape evolution characterization — to provide a contextual framework for the transport history of the alluvial nuggets, for the purpose of locating their primary source. This component was carried out by GSWA and KGM geologists. It comprised field validation and interpretation of existing detailed, large-scale (1:10 000), open-file geological mapping completed by exploration companies (e.g. Schupp, 1985a,b), supplemented with profile mapping in trenches or other excavations undertaken by KGM at selected sites.

Gold grain characterization — grain morphology, microstructure, trace-element chemistry, micro-inclusion and gangue mineralogy of gold. The small gold nuggets were recovered from regolith and evaluated using techniques that included visual morphometry, acid etching, reflectance microscopy, scanning electron microscopy with energy dispersive X-ray analysis (SEM-EDX), and laser ablation inductively coupled plasma mass spectrometry (LA-ICP-MS).

A significant outcome from this study is the development of a technique for **quantitative** determination of the trace-

element chemistry of gold using LA-ICP-MS. GSWA contracted TSW Analytical, the only laboratory in Australia with the capability and experience to undertake the desired microchemical studies, and which presently offers semiquantitative chemical analysis of gold (Watling et al., 1994). GSWA geologists worked with TSW Analytical staff firstly to validate the reported trace-element compositions of two certified commercial gold standards purchased for this project, hence to characterize the compositions of the Kurnalpi specimens. Similar work on gold standard validation and application for placer gold has been performed in the central Okanagan (Canada) by Tetland (2015) using only one gold standard.

Mineral inclusion and gangue mineral characterization were performed using optical microscopy and SEM-EDS analysis.

Geological setting

The Kurnalpi goldfield is located about 85 km east-northeast of Kalgoorlie in the Kurnalpi Terrane of the Eastern Goldfields Superterrane (Fig. 1). The field was discovered in 1894, and is renowned for its 'alluvial' gold, producing early in its history large nuggets exceeding 200 oz (approximately 6.2 kg; Montgomery, 1905; Jutson, 1914). Alluvial gold is associated with Quaternary detrital deposits, Cenozoic laterite and calcrete deposits, and pre- or early Cenozoic deep leads in buried paleochannels (Schupp, 1985a). Some gold was mined from bedrock, mostly from quartz veins along narrow shear zones cutting basalt, or at the contacts between felsic, mafic and/or ultramafic rocks. Higher grade gold zones are located at the intersection between lenticular, randomly oriented, narrow quartz veins and also correspond with hematite 'indicators' of uncertain affinity (Jutson, 1914).

Total recorded gold production for the Kurnalpi goldfield is 7187.94 oz (223.58 kg), comprising 3175.2 oz (98.76 kg) of 'dollied' (= crushed 'alluvial'?) material, and 4013.0 oz (124.82 kg) classified as 'ore' (= bedrock derived?) material. These gold production figures are likely to be minimum estimates considering that production records for the area are incomplete. For example, alluvial gold discoveries are probably under-reported to the extent that thousands of ounces were likely extracted from the goldfield since the mid-1980s when Metana Minerals undertook alluvial production test work (Schupp, 1985 c–e; Schupp, 1986 a,b).

Prospectors continue to win placer gold from the goldfield, focusing on thin gravels at the base of Quaternary channels, buried 1–2 m below the present surface beneath surficial loams (the loams themselves appear to be barren of gold). More extensive, but still subeconomic, bedrock-hosted gold mineralization was defined at the Scottish Lass and Brilliant prospects (Fig. 1). Gold in these prospects is microscopic and hosted by moderately dipping quartz veins, with associated quartz–pyrite±carbonate±hematite alteration in metabasalt, or north-northwesterly striking, magnetite-bearing, granophyric quartz dolerite dykes less than 20 m wide that cut ultramafic rocks (Swager, 1994; Steuart, 2001; Gunther, 2004; Johnson, 2014).

Gold mineralization at the Scottish Lass and Brilliant prospects is similar in its physical and chemical characteristics to other quartz vein stockwork deposits in the Eastern Goldfields Superterrane (e.g. Darlot; Beardsmore and Gardner, 2003); however, it is unclear whether these prospects are the main hypogene source for the more coarsely grained, placer gold nuggets discovered in the Kurnalpi goldfield. Surficial inorganic or biogenic processes are proposed as additional mechanisms for the formation of gold nuggets (e.g. Wilson, 1984).

The basement geology of the Kurnalpi goldfield comprises folded Archean ultramafic, mafic, intermediate and acidic extrusive volcanic rocks, and intrusive granitic rocks that are cut by north-northwesterly trending, west-dipping shear zones, and younger northeasterly trending faults (Swager, 1994). Bedrock crops out in two north-trending series of hills of low to moderate relief. The hills transition laterally into wide, alluvial valleys that drain to the south into Lake Yindarlgooda, which is a Cenozoic paleochannel comprising fluvial and lacustrine sediments.

Detrital zones in the Cenozoic regolith are up to 40 m thick, and preserve the history of weathering, erosion and landscape development. Alluvial gold was probably mobile throughout this history, and gold in Quaternary deposits may in part have been remobilized from older channel deposits; many shallow historical alluvial gold workings lie adjacent to, or within, cemented ferruginous pisolitic caps on low hills, which might be relics of once-buried Eocene channels now exhumed by erosional inversion (Schupp, 1985a).

The Yilgarn Craton was extensively glaciated during the early Permian and was at least locally incised by subglacial channels (Eyles and de Broekert, 2001). The possible influence of Permian glaciation on dispersal of gold in the Eastern Goldfields Superterrane is not known, but the preservation of the glacial features does suggest that there has been little further erosional stripping of Archean basement since at least the early Permian. If alluvial gold in Cenozoic sediments was liberated from bedrock sources, at least part of these original deposits should therefore still remain in the bedrock, awaiting discovery.

Methodology

Sampling

GSWA examined and photographed a suite of 274 (389.9 g) gold nuggets from 37 sites distributed across the Kurnalpi goldfield. Due to time and cost restrictions, 75 (169.4 g) representative samples were selected from the initial suite for further analysis (Appendix 1). Gold nuggets were selected based on their degree of roundness, in such a way to show the greatest variation in this physical property and the greatest spatial coverage in the Kurnalpi goldfield. In the case of the well-rounded nuggets (e.g. GSWA 201948), the grains were separated into groups by their size and extracted for analyses accordingly. Ownership of the selected samples passed to GSWA at the completion of the project.

Mineralogical analyses

The mineralogical method used in this study is described by Hancock and Thorne (2011). All gold nuggets were first

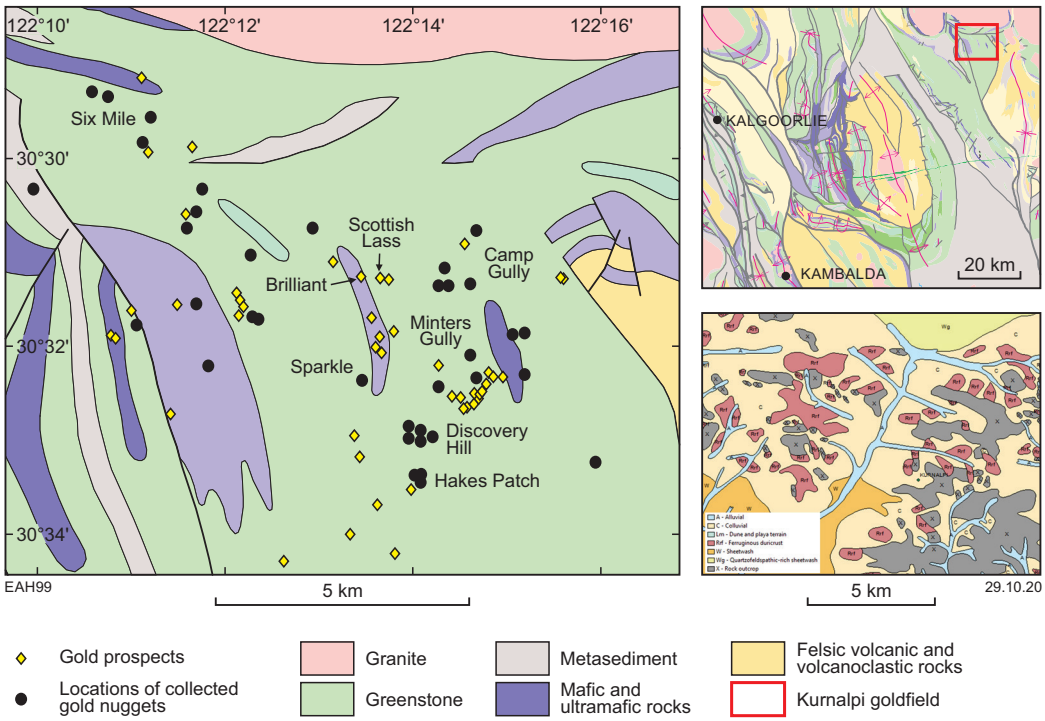

Figure 1. Solid geology interpretation for the Kurnalpi Goldfield, showing local gold prospects and location of gold nuggets. Insert: regional geology map with study area in red rectangle, and summary surface geology map for study area. Bedrock and surface geology from Martin et al. (2016)

photographed and weighed, and their gross morphology and external features, such as colour, roundness, surface relief, coatings, mineral inclusions, and mineralogical assemblages were recorded using visual morphometry, optical and electron microscopy (Appendix 1). The gold nuggets were mounted in epoxy resin, cut and polished in CSIRO's sample preparation laboratory in Kensington, Perth. From the selection of 75 gold nuggets, 35 specimens from 19 sites (GSWA 201929–201947) were analysed using the full gamut of the before-mentioned analytical techniques. Gold surfaces were repolished after laser ablation traverses. An additional 23 (two small grains were lost during polishing) gold nuggets chosen from proximal localities to potential primary sources (from the following GSWA sample sites: 201949, 201950, 201954, 201955, 201956, 201957, 201958, 201960, 201962, 201964) were characterized for Ag and trace-element contents and mineral inclusions using SEM-EDX and LA-ICP-MS. No further work was performed on these specimens (i.e. repolishing and the final acid etching analysis) owing to the lack of significant variations in their microstructure observed during Back-Scattered Electron (BSE) imaging. The remaining 15 gold nuggets from the GSWA collection were only described in terms of their morphology and external features (Appendix 1).

SEM-EDS analysis

Silver content of the gold nuggets and identification of associated minerals and inclusions were analysed using CSIRO's Philips XL-40 SEM-EDS. In addition, high-resolution BSE was used for preliminary observation of gold microstructures. It was noted that some optically contrasted internal features, such as high-purity intergranular veinlets, could be observed using reflectance microscopy.

The electron back-scattered diffraction (EBSD) detector was used to map crystallographic orientations of two gold nuggets. Data were obtained from the Tescan Mira3 Variable Pressure Field Emission SEM (VP-FESEM) at the John de Laeter Centre, Curtin University. Prior to EBSD analysis, gold grain surfaces were etched using CSIRO's Ion Beam Milling (IBM) technique.

For Ag analysis, the SEM-EDS was originally calibrated using the carbon-coated CSIRO Au80Ag20 standard.

LA-ICP-MS analysis

All polished gold samples were analysed for their chemical composition at the TSW Analytical laboratory using a New Wave UP213 Laser Ablation unit coupled to an Agilent Technologies 7500c LA-ICP-MS. Trace-element analyses were determined by calibration against certified gold reference materials (CRM), AuRM1 and AuRM2, provided by the London Bullion Metals Association (LBMA), and standard produced by the Perth Mint. The homogeneity of these gold standards was validated through analysis by TSW Analytical (Appendix 2) to investigate the suitability of the LA-ICP-MS method for the quantitative analysis of the gold samples. The advantages of using the gold standards are that quantitative data (in parts per million — ppm) are reproducible and can be used to compare gold compositions between different studies. This contrasts with data reported in relative values (counts per second — cps) commonly used as ratios for gold forensic analysis (Watling et al., 1994).

The quantitative LA-ICP-MS method was applicable for 22 elements presented in AuRM1, AuRM2, and JWAu standards: Ag, Al, As, Bi, Ca, Cr, Cu, Fe, Mg, Mn, Ni, Pb, Pd, Pt, Rh, Sb, Se, Si, Sn, Te, Ti and Zn. For other elements that do not have certified concentrations from standards, semiquantitative results are reported as cps data (e.g. Hg). The obvious spikes in the analytical data caused by impurities/inclusions were removed during data reduction, while residual mean elemental values in cps measured along the traverses were calibrated against their certified values. Repeat analyses of the standards facilitated the calculation of the standard deviation for each element in each standard. Calibration graphs were produced for the elements in AuRM1 and AuRM2. Also, where data are available, the graphs incorporated concentrations for the JWAu standard. The results show excellent correlations for all elements except Pt; hence, the standards are considered suitable for quantitative LA-ICP-MS analysis of trace elements in native gold on the gross scale.

However, heterogeneity in the distribution of trace elements in the certified gold reference standards is evidence of partial exsolution and concentration of trace elements along gold crystal lattice occurred during sample preparation (Hancock et al., 2017). This premise was investigated using EBSD analysis of deeply cleaned surface of AuRM2 gold standard. EBSD crystallography revealed matted, strongly damaged multicrystalline microstructure (Fig. 2a), which illustrates standard preparation through blending and stirring of gold melt, and rolling of quenching cast into a thinner sheet (Murray, 2009). Deeper cleaning of the standard surface using IBM etching does not show different results (Fig. 2b).

Another complication in the quantitative chemical analysis of gold grains is the very low Ag content (<100 ppm) in the gold standards, which produces calibration and calculation variations for native gold samples with Ag concentrations in percentage levels. For this reason and semiquantitative SEM-EDS data, there are some mismatches in Ag contents analysed by two instruments (Fig. 3). However, it must be highlighted, that currently, without relevant high-content Ag standard (in %), any LA-ICP-MS data for Ag are treated as semiquantitative.

According to the developed analytical protocol, all gold samples were ablated for 60 seconds with 10 Hz frequency and 100 µm diameter of laser spots size producing a traverse of about 1.3 mm in length. All samples were ablated in triplicate and average data for each element per traverse are presented in Appendix 3.

Acid etching

Traditional acid etching at room temperature was used in this study to determine the internal crystal structure of gold samples (Nikolaeva et al., 2004). The reaction time between aqua regia and gold varied from 10 seconds to a minute, depending on the amount of effort required to remove the smeared (Beilby) layer from the polishing surface and the initial etching of gold crystal lattice. Aqua regia is commonly used to reveal polycrystalline fabrics and twinning in gold. Ten gold samples were then repolished and etched with CrO_3 in HCl solution for a few seconds to promote a reaction with Ag on the surface of the gold nuggets so as to reveal possible compositional zoning.

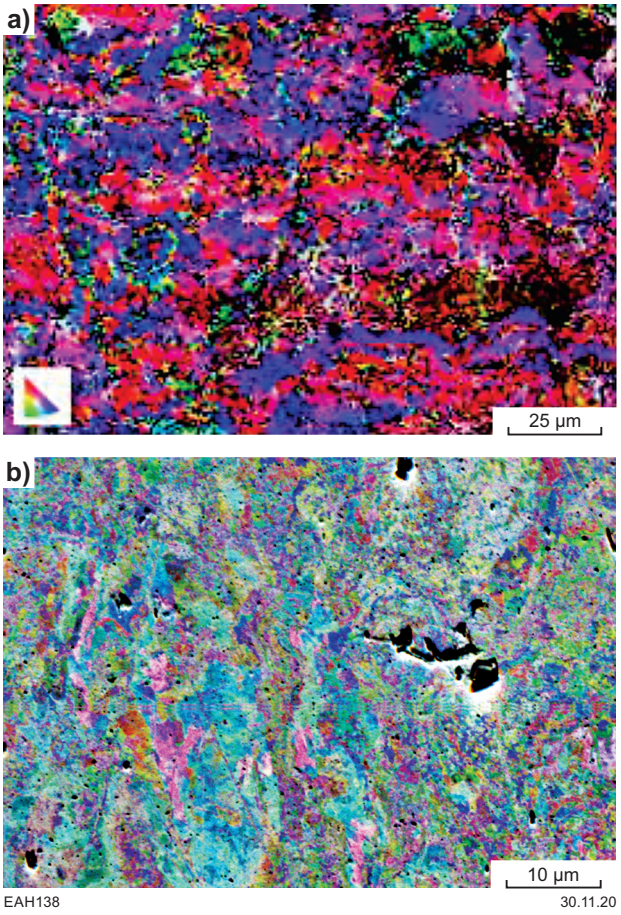

Figure 2. Electron back-scattered diffraction (EBSD) images of the polished surface of gold standard AuRM2 showing muddle, strongly damaged multicrystalline microstructure: a) initially polished with diamond paste; b) deeper etched using Ion Beam Milling (IBM)

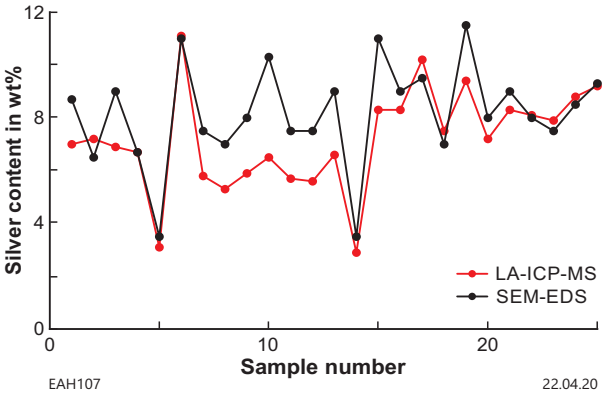

Figure 3. Silver contents in gold nuggets measured by SEM-EDS and LA-ICP-MS

Results

Morphometry

The size of 274 gold nuggets presented to GSWA varies between 4 and 25 mm and the weight ranges from 0.3 to 18.8 g. The largest nugget is 25 x 20 x 15 mm and weighs 18.8 g (Appendix 1).

The gold samples from each site were visually separated into groups according to their degree of roundness (Nikolaeva et al., 2004):

- Non-rounded or angular
- Slightly rounded
- Subrounded
- Medium rounded
- Well rounded
- Perfectly rounded or plates.

The last group refers to fine, flattened gold plates and spherical gold grains that were modified in the supergene environment due to their significant alteration and transportation away from the primary mineralization source. Only 10 samples from the available 274 nuggets were allocated to this group, including one from Spud Flat (GSWA 201946; Fig. 4a), six from an area located southwest from Sparkle (GSWA 201949), and three from the Lower Italian Gully (GSWA 201960).

By contrast, the first three morphological groups are considered to show low abrasion or alteration and indicate a proximal location to their primary source. They are accordingly used as reference materials for the mineralogical and geochemical signatures of primary mineralization in the area. The samples include:

- GSWA 201930, Six Mile, four nuggets
- GSWA 201941 and 201942, Camp Gully, six nuggets
- GSWA 201947 and 201962, Minters Gully, three nuggets
- GSWA 201949, southwest from Sparkle, one nugget
- GSWA 201950 (Fig. 4b), 201951, and 201954, southwest from Discovery Hill, more than 50 nuggets
- GSWA 201955, 201956 and 201957, Hakes Patch, nine nuggets.

Unfortunately, prior to this study following their collection some gold nuggets were cleaned with an acid to dissolve surface inclusions and coatings, with the aim of enhancing their aesthetically pleasing metallic lustre. As a result, some mineralogical and surface chemistry information (depending on the acid concentration and cleaning time) could have been lost or changed. Despite this challenge, the following intergrowths and gangue minerals were observed:

- Quartz — large milky and grey crystals are intergrown with gold; small grains are mixed with ferruginous clays in cavities located within the gold surface
- Maghemite — large grains/crystals are present in gold as massive segregation-filled cavities, voids and intergranular veinlets. Maghemite was formed by oxidation of magnetite at >50°C (during bushfire) and it is stable at surface conditions. Note that magnetite-bearing, granophyric dolerite is well known in the area
- Carbonates — fine grains are mixed with clays within surficial cavities in gold; also present as small calcite crystals in intergranular veinlets
- Ilmenite grains fill cavities and large veinlets in gold nuggets. Ilmenite and pseudo-rutile are intergrown with one of the gold nuggets
- Ferruginous coatings exist on some gold surfaces while Fe oxides occur with clay minerals in surficial cavities and in intergranular veinlets. Note that quartz–pyrite±carbonate±hematite alteration is reported in association with gold mineralization in the area.

Currently all described gangue minerals, except intergrown with gold, are interpreted to be the product of accretionary cementation during lateritic weathering (Anand and Butt, 2010). However, more study is recommended for any conclusions related to the genesis of gold nuggets.

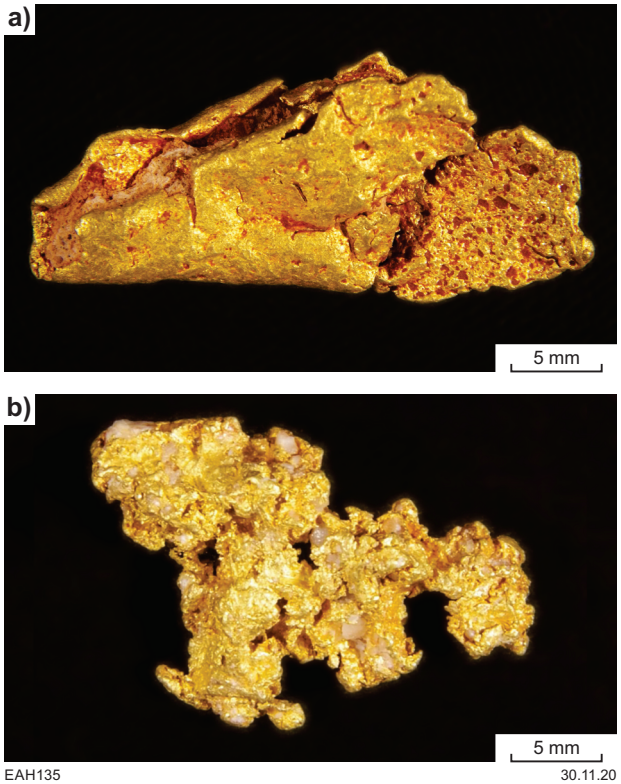

Figure 4. Morphology of gold nuggets: a) strongly deformed sample representative of about 5% of the gold collection: highly rounded, folded and flattened with ferruginous clay inclusions, GSWA 201946; b) residual primary sample representing about 30% of the collection: angular, irregular, spongy intergrown with quartz, GSWA 201950

Mineral micro-inclusions

Mineral micro-inclusions identified by SEM-EDS include Ag, Au, Pb, and Bi-bearing tellurides, arsenopyrite, pyrite, chalcopyrite and galena. Inclusions of Ag–(Au) tellurides are present in about 20% of the nuggets. They are 10–100 µm in size and typically located on the side of larger rounded cavities. Lead and Bi tellurides (altaite, PbTe; tellurobismuthite, Bi_2Te_3; and tetradimite, Bi_2Te_2S) were observed in samples GSWA 201949 and 201956. They are rounded or curved and 50–150 µm in diameter (Fig. 5a). Arsenopyrite inclusions presented in one gold nugget (GSWA 201930; Fig. 5b) are <100 µm and mostly rounded. A 50 µm chalcopyrite inclusion and a potassium silicate mineral are present in sample GSWA 201937. Rounded galena inclusions are 50–400 µm in samples GSWA 201935, 201941 (Fig. 5c), 201943 and 201949. Cu–Pb–Bi and Ag–Te mineral phases are locally present within galena.

Locally developed, large veinlets in the gold nuggets are filled with fine-grained, pure gold particles and, together with ferruginous clay, they define a spongy-like texture (Fig. 5a). Spherical cavities in some nuggets are potentially the result of dissolution of mineral inclusions, or represent preserved gas bubbles that formed during the boiling of supersaturated hydrothermal fluids.

Silver and trace elements

Silver concentration determined by LA-ICP-MS and SEM-EDS is consistent in most samples, ranging from 3 to 12 wt% (Table 1). The average data from LA-ICP-MS are lower (Fig. 3) and are likely related to the very low concentration of Ag in the gold standards.

Silver content as low as 3 wt% is in spongy-like gold nuggets from samples GSWA 201930, 201938 and 201950. Three solid, semicrystalline nuggets (GSWA 201931, 201940 and 201942) delivered a higher Ag content of ~10–12 wt%. These observations were independently confirmed by the LA-ICP-MS and SEM-EDS methods.

In addition to Ag, only Cu and Hg are present in concentrations that are consistently above the detection limit for the LA-ICP-MS technique (Table 2). Tellurium, Pb, Bi, Al, Fe and Mg are present in concentrations above the detection limit in a few samples. Antimony, Sn, As, Zn, Rh, Pd, Pt, Ti, Cr, Mn and Ni contribute to the counts per second results, but their quantitative values are lower than their standard deviations; hence, these elements are not discussed further.

In general, the distribution of the detectable trace elements is relatively uniform across the laser traverses (e.g. GSWA 201941; Fig. 6a). However, where the sample's microstructure is heterogeneous, the data in the table are reported separately for the individual phases (e.g. GSWA 201929; Fig. 6b).

In order to validate the LA-ICP-MS results and to understand variations between spot/traverse and bulk gold analyses, small parts from three gold nuggets (GSWA 201936, 201938 and 201944) were cut, dissolved, and their solutions were analysed by ICP-MS. As expected, lithophile elements, which are present in the samples

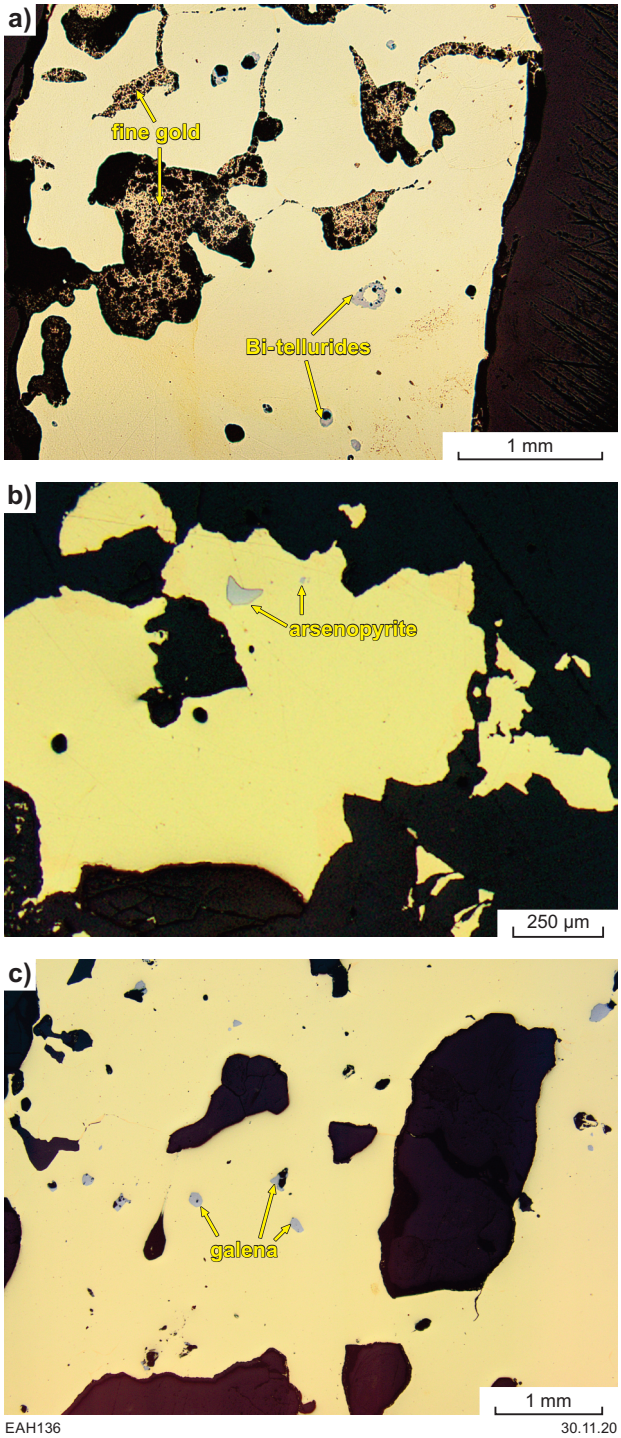

Figure 5. **Reflected light photomicrograph of cut and polished gold nuggets showing mineral inclusions of: a) spongy-like fine secondary gold in well-developed voids and veinlets, and partly leached Bi-tellurides (grey), GSWA 201949; b) arsenopyrite, only in sample GSWA 201930; c) rounded, partly leached galena, GSWA 201941**

Table 1. LA-ICP-MS data of Ag weight percentage mean per traverse

GSWA sample no.	*Gold nugget no.*	*Ag, wt%, mean per traverse*
201929	1	5.0, 5.4, 6.5, 6.9, 8.6, 9.4
	2	5.2, 6.1, 6.5
	3	6.4, 7.2, 8.1
201930	1	6.9, 6.9, 6.9, 7.0, 7.0
	2	6.4, 6.7, 7.1
	3	3.0, 3.0, 3.3
201931	1	6.9, 7.2, 8.6, 8.9
	2	10.1, 11.2, 11.3, 11.7
201932	1	6.9, 7.0, 7.8
201933	1	4.6, 4.8, 5.0
	2	5.1, 5.2, 7.1
	3	4.7, 4.9, 5.5, 6.1
201934	1	5.0, 6.0, 6.6
201935	1	5.1, 5.5, 5.9
	2	5.7, 6.4, 7.3
201936	1	5.3, 5.8, 5.9
	2	5.1, 5.9, 5.9
201937	1	5.7, 6.6, 7.5
	2	5.7, 6.0, 6.6
201938	1	2.2, 2.4, 2.6
	2	2.7, 3.0, 3.0
201939	1	6.5, 6.7, 6.7
	2	8.3, 8.3, 8.4
201940	1	7.6, 8.0, 9.4
	2	9.4, 9.8, 11.3
201941	1	7.0, 7.3, 8.2
201942	1	8.9, 9.5, 9.8
201943	1	6.8, 7.1, 7.6
201944	1	8.0, 8.3, 8.6
201945	1	7.2, 7.8, 9.2
201946	1	7.5, 8.1, 8.2
201947	1	8.6, 8.8, 9.0
	2	9.1, 9.1, 9.3
201949	1	3.9, 4.1, 5.4
	2	5.1, 5.4, 5.5
	3	5.2, 5.4, 5.9
	4	7.0, 7.0, 7.3
	5	4.6, 5.0, 5.0
	6	5.6, 5.6, 5.8
201950	1	3.1, 3.3, 3.9
201954	1	4.6, 5.3, 5.4
201955	1	4.8, 5.0, 5.1
	2	3.9, 4.0, 4.1
	3	4.2, 4.2, 4.3
	4	4.6, 4.6, 4.7
201956	1	5.5, 5.9, 7.0
	2	4.5, 4.8, 5.1
201957	1	4.9, 5.1, 6.2
201958	1	4.3, 5.1, 5.6
201960	1	3.6, 3.9, 4.4
	2	3.2, 3.8, 5.6
	3	5.3, 5.3, 5.8
201962	1	3.4, 3.6, 4.3
	2	4.6, 4.7, 5.2
201964	1	5.3, 6.2, 6.7
	2	3.7, 3.7, 3.8

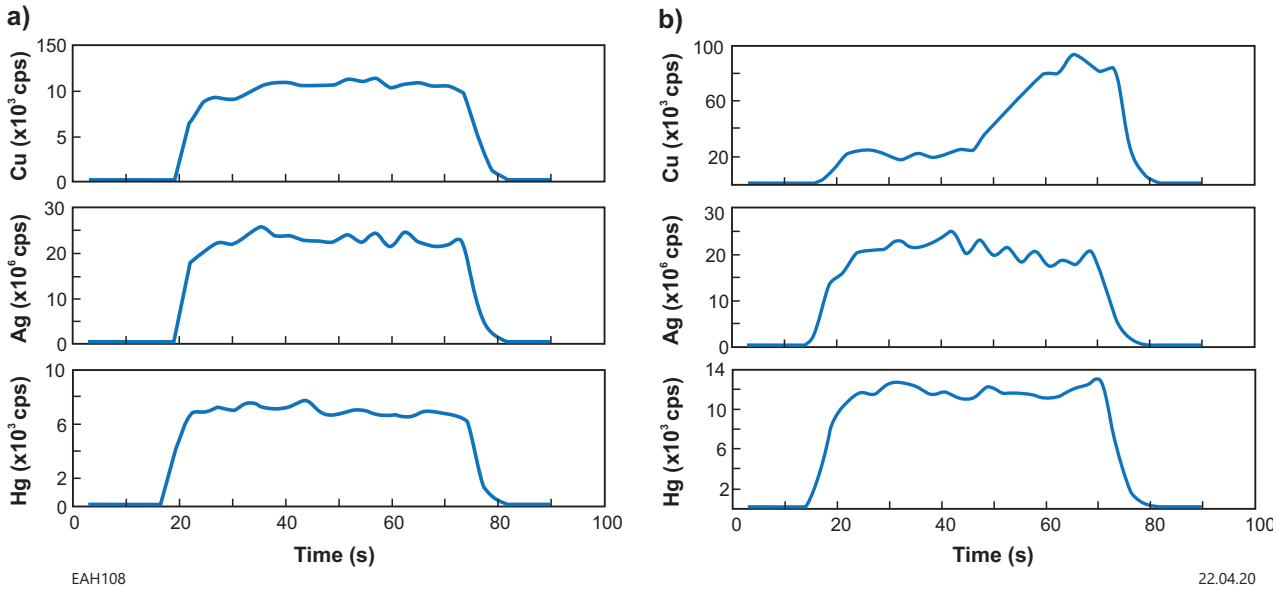

Figure 6. LA-ICP-MS data for the distribution of Cu, Ag and Hg across two traverses on the surface of a cut and polished gold nugget: a) relatively homogeneous distribution of all elements, sample GSWA 201941, nugget 1, line 1; b) heterogeneous distribution of Cu and Ag showing two phases of Cu and wavy pattern of Ag due to structural variations (polysynthetic twinning in high Cu phase), sample GSWA 201929, nugget 2, line 3

as mineral inclusions of the surrounding regolith, were detected and are more abundant relative to their respective laser ablation traverse data (Table 3). In addition, the concentration of chalcophile elements, such as Ag, Cu and Hg, are elevated when measured in solution due to a higher proportion of mineral inclusions in gold.

Microstructure

The following gold microstructural features were observed:

- Polycrystalline fabrics of gold aggregates and intergranular veinlets (GSWA 201937; Fig. 7a)
- Polysynthetic and simple twinning, coherent and incoherent (GSWA 201930; Fig. 7b)
- Diffusive zoning (GSWA 201947; Fig. 7c):
- Silver diffusion zones and recrystallized rims (GSWA 201937; Fig. 7d)
- Partial recrystallization (GSWA 201930; Fig. 7e)
- Recrystallization and initial disintegration and granulation (GSWA 201931; Fig. 7f)
- Recrystallization around mineral inclusions (GSWA 201934; Fig. 7g)
- Intensive intergranular veinlets and voids filled with fine-grained pure (secondary) gold (GSWA 201931; Fig. 7h).

The verification of gold microstructures traditionally revealed by acid etching, was conducted using modern EBSD analyses and prior cleaning by IBM etching. An example is demonstrated on two gold nuggets from Minters Gully (GSWA 201962). They revealed monocrystalline and polycrystalline microstructures, with polysynthetic twinning in a recrystallized rim (Fig. 8).

Discussion

A combination of gold morphometry, mineral inclusions, Ag and trace-element contents, and microstructure of gold nuggets are used here to interpret primary mineralization sources in the Kurnalpi goldfield and evaluate their mineralization type.

Characterization of gold nuggets located proximal to primary mineralization

Although all gold nuggets were collected in regolith 1–2 m below the present surface and correspond to the base of Quaternary paleochannels, their morphological characteristics suggest that about 30% of the studied nuggets were found close to their primary mineralization source (Table 4). These nuggets have angular, irregular, and only slightly rounded shapes, with the preservation of delicate crumpling of individual ledges on their surfaces indicating limited physical reworking. Some nuggets display a typical bedrock gold appearance, such as intergrowths with milky quartz, and shiny, even or spongy surfaces. Other nuggets are free from quartz and, with respect to the regolith mineralogy, have variable brown ferruginous or white carbonate–clay coatings. Silver contents vary from 3% in spongy nuggets from the Six Mile and Discovery Hill areas to 9–11 wt% in the more irregular-shaped and semicrystalline nuggets from the Camp Gully and the Minters Gully areas. By contrast, Cu and Hg do not show significant variations between nuggets (i.e. 30–150 ppm for Cu and 10–100 ppm for Hg), only copper is slightly elevated (up to 200–300 ppm) in the Six Mile and the Camp Gully areas. Other trace elements that are noticeably present in gold from these areas include Sb and Pb and, possibly due to the local incorporation of regolith material, Al, Fe and Mg.

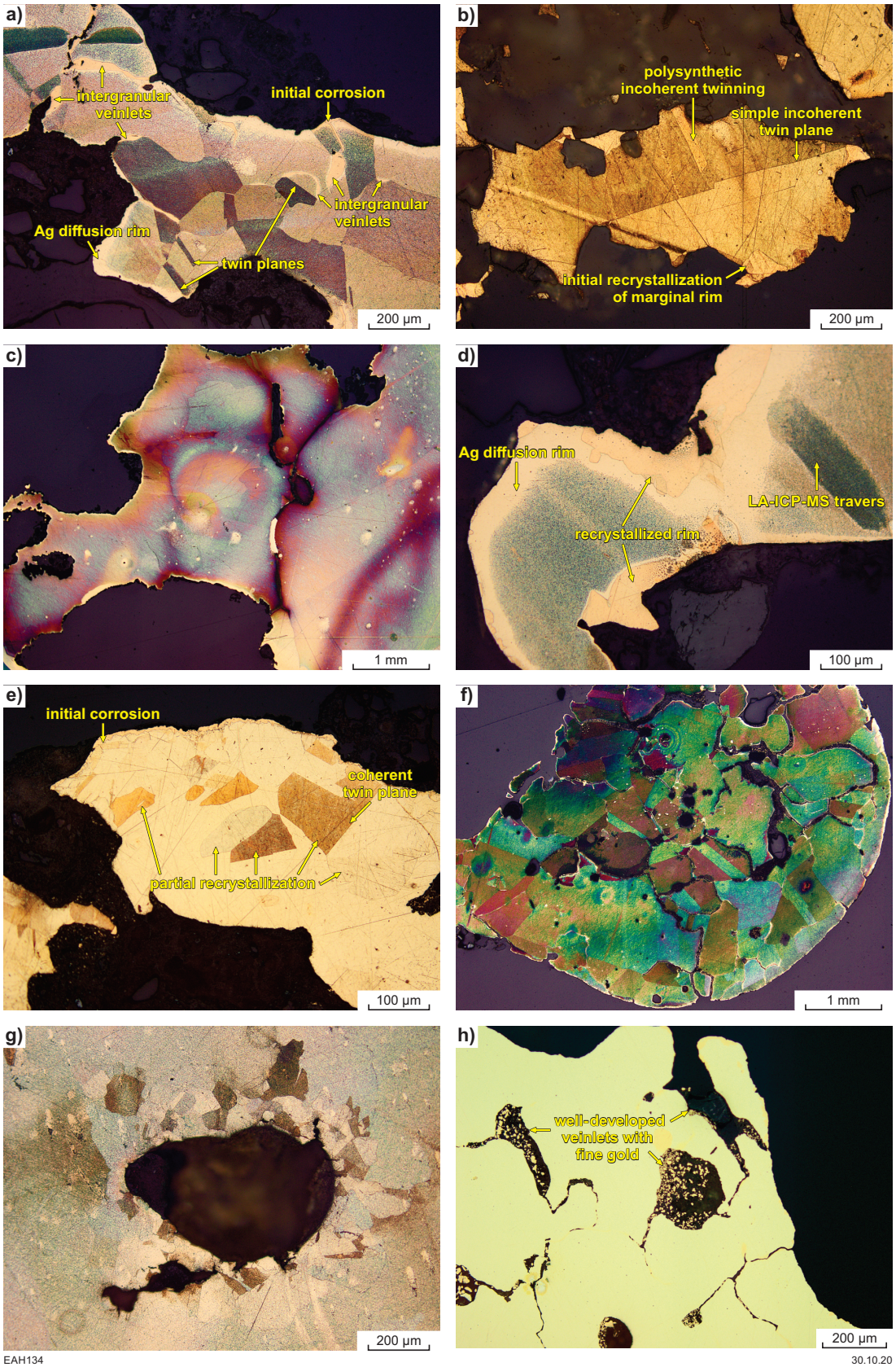

Figure 7. Reflected light photomicrographs of cut, polished and acid etched gold nuggets showing their microstructure: a) polycrystalline partly recrystallized fabric with high-purity intergranular veinlets, twinned planes, Ag diffusion rim, and initial corrosion, GSWA 201937; b) simple and polysynthetic incoherent twinning, initial recrystallization of marginal rim, GSWA 201930; c) diffusive zoning, GSWA 201947; d) Ag diffusion zones and pure gold recrystallized rim, GSWA 201937; e) partial hypogenic recrystallization and initial corrosion, GSWA 201930; f) recrystallization and initial disintegration and granulation, GSWA 201931; g) recrystallization around mineral inclusions, GSWA 201934; h) well-developed large veinlets in the gold nugget filled with numerous fine-grained, pure gold particles together with silica and ferruginous clay, forming spongy-like texture, GSWA 201931

Table 2. LA-ICP-MS data of trace elements in gold nuggets in ppm mean per traverse

GSWA sample no.	Nugget no.	Traverse line	Cu	Sb	Te	Hg	Pb	Bi
201929	1	1	545.8	0.0	0.0	143.2	0.0	0.0
201929	1	2	480.9	0.0	0.0	118.0	0.0	0.0
201929	1	2	430.4	0.0	0.0	110.0	0.0	0.0
201929	2	1	229.4	2.2	0.0	37.1	0.0	0.0
201929	2	2	223.4	0.0	0.0	38.9	0.0	0.0
201929	2	3 Phase 1	39.1	0.0	0.0	717.0	0.0	0.0
201929	2	3 Phase 2	134.6	0.0	0.0	710.1	0.0	0.0
201929	2	4	173.4	2.3	0.0	31.1	0.0	0.0
201929	2	5	185.3	0.0	0.0	37.4	0.0	0.0
201929	3	1	135.6	0.0	0.0	465.7	0.0	0.0
201929	3	2 Phase 1	39.4	0.0	0.0	515.8	0.0	0.0
201929	3	2 Phase 2	17.5	0.0	0.0	528.2	0.0	0.0
201930	1	1	177.1	0.0	0.0	55.6	0.0	0.0
201930	1	2	238.0	0.0	0.0	80.1	0.0	0.0
201930	1	2 Phase 1	205.1	0.0	0.0	69.1	0.0	0.0
201930	1	2 Phase 2	163.0	0.0	0.0	65.7	0.0	0.0
201930	2	1	220.8	0.0	0.0	117.2	0.0	0.0
201930	2	2	265.8	0.0	0.0	93.6	0.0	0.0
201930	2	3	243.5	0.0	0.0	84.1	0.0	0.0
201930	3	1	274.8	0.0	0.0	40.2	0.0	0.0
201930	3	2	295.7	0.0	0.0	42.7	0.0	0.0
201930	3	3	293.2	0.0	0.0	41.5	0.0	0.0
201931	1	1	310.2	0.0	101.2	9.6	0.5	198.3
201931	1	2	230.5	0.0	19.0	7.3	0.0	9.6
201931	1	3	142.6	0.0	0.0	6.5	0.0	0.0
201931	2	1	73.3	0.0	0.0	151.1	0.0	0.0
201931	2	2	81.8	0.0	0.0	201.1	0.0	0.0
201931	2	3 Phase 1	69.3	0.0	0.0	209.2	0.0	0.0
201931	2	3 Phase 2	45.6	0.0	0.0	192.0	0.0	0.0
201931	2	3 Phase 3	71.5	0.0	0.0	183.5	0.0	0.0
201932	1	1	91.9	0.0	0.0	40.1	0.0	0.0
201932	1	2	87.5	0.0	0.0	59.9	0.0	0.0
201932	1	3	104.8	0.0	0.0	97.3	0.0	0.0
201933	1	1	312.0	0.0	0.0	53.7	0.0	0.0
201933	1	2 Phase 1	126.2	0.0	0.0	72.8	0.0	0.0
201933	1	2 Phase 2	240.6	0.0	0.0	67.6	0.0	0.0
201933	1	3	174.0	0.0	0.0	55.2	0.0	0.0
201933	2	1	332.6	0.0	0.0	46.4	0.0	0.0
201933	2	2	271.3	0.0	0.0	36.3	0.0	0.0
201933	2	3	263.6	0.0	0.0	34.3	0.0	0.0
201933	3	1	235.1	0.0	0.0	78.5	0.0	0.0
201933	3	2	217.2	0.0	0.0	79.7	0.0	0.0
201933	3	3	240.2	0.0	0.0	75.7	0.0	0.0
201934	1	1	205.9	0.0	0.0	39.5	0.0	0.0

Table 2. continued

GSWA sample no.	Nugget no.	Traverse line	Cu	Sb	Te	Hg	Pb	Bi
201934	1	2	245.9	0.0	0.0	52.9	0.0	0.0
201934	1	3	234.7	0.0	0.0	48.7	0.0	0.0
201935	1	1	171.7	0.0	0.0	10.8	0.0	0.0
201935	1	2	195.3	0.0	0.0	11.7	0.0	0.0
201935	1	3	163.7	0.0	0.0	13.2	0.0	0.0
201935	2	1	95.7	0.0	0.0	9.2	0.0	0.0
201935	2	2	97.4	0.0	0.0	11.5	0.0	0.0
201935	2	3	129.7	0.0	0.0	13.5	0.0	0.0
201936	1	1	159.6	0.0	0.0	71.2	0.0	0.0
201936	1	2	125.2	0.0	0.0	94.2	0.0	0.0
201936	1	3	122.4	0.0	0.0	90.5	0.0	0.0
201936	2	1	189.9	0.0	0.0	66.4	0.0	0.0
201936	2	2	191.4	0.0	0.0	65.2	0.0	0.0
201936	2	3	163.5	0.0	0.0	54.0	0.0	0.0
201937	1	1	144.9	0.0	0.0	70.8	0.0	0.0
201937	1	2	137.0	0.0	0.0	80.6	0.0	0.0
201937	1	3	176.7	0.0	0.0	92.4	0.0	0.0
201937	2	1	137.0	0.0	0.0	80.6	0.0	0.0
201937	2	2	246.8	0.0	0.0	15.9	0.0	0.0
201937	2	3	192.1	0.0	0.0	18.2	0.0	0.0
201938	1	1	260.4	0.0	0.0	4031.8	0.0	0.0
201938	1	2	266.8	0.0	0.0	4260.8	0.0	0.0
201938	1	3	415.0	0.0	0.0	3814.8	0.0	0.0
201938	2	1	552.8	0.0	0.0	223.3	0.0	0.0
201938	2	2	502.2	0.0	0.0	192.3	0.0	0.0
201938	2	3	585.0	0.0	0.0	212.3	0.0	0.0
201939	1	1	136.6	0.2	0.4	10.2	0.0	0.0
201939	1	2	139.3	0.3	0.4	10.2	0.0	0.0
201939	1	3	131.4	0.2	0.3	10.8	0.0	0.0
201939	2	1	293.3	1.5	0.3	1.2	0.0	0.0
201939	2	2	304.0	1.4	0.3	1.0	0.0	0.0
201939	2	3	297.5	1.4	0.3	0.9	0.0	0.0
201940	1	1	95.2	7.3	0.4	31.8	0.0	0.0
201940	1	2	97.2	8.3	0.2	23.7	0.0	0.0
201940	1	3	109.6	8.8	0.4	25.5	0.0	0.0
201940	2	1	197.0	0.4	0.5	5.6	0.0	0.0
201940	2	2	180.2	0.4	0.4	5.1	0.0	0.0
201940	2	3	183.2	0.4	0.5	5.1	0.8	0.3
201941	1	1	236.6	0.1	0.4	11.4	0.5	0.1
201941	1	2	184.8	0.1	0.3	9.8	0.0	0.0
201941	1	3	146.4	0.0	0.2	10.5	0.0	0.1
201942	1	1	133.9	0.3	0.3	18.1	0.0	0.1
201942	1	2	109.4	0.4	0.3	41.4	0.0	0.0
201942	1	3	125.0	0.4	0.3	19.7	0.0	0.0

Table 2. continued

GSWA sample no.	Nugget no.	Traverse line	Cu	Sb	Te	Hg	Pb	Bi
201943	1	1	149.8	0.0	0.3	3.7	0.0	0.0
201943	1	2	166.9	0.0	0.3	4.3	0.0	0.0
201943	1	3	161.0	0.0	0.3	4.0	0.0	0.0
201944	1	1	112.0	0.3	0.3	13.3	0.0	0.0
201944	1	2	149.9	1.3	0.3	10.6	0.0	0.0
201944	1	3	161.1	1.1	0.3	11.1	0.0	0.0
201945	1	1	185.5	0.0	0.3	14.4	0.0	0.0
201945	1	2	134.2	0.0	0.2	13.6	0.0	0.0
201945	1	3	219.6	0.0	0.3	14.1	0.0	0.0
201946	1	1	177.6	0.0	0.2	6.1	0.0	0.0
201946	1	2	182.0	0.1	0.3	5.4	27.6	0.6
201946	1	3	182.8	0.0	0.3	6.1	0.7	0.0
201947	1	1	143.2	0.2	0.2	59.8	0.0	0.0
201947	1	2	126.4	0.2	0.2	55.2	0.0	0.0
201947	1	3	135.0	0.2	0.3	67.4	0.0	0.0
201947	2	1	169.4	0.0	0.3	11.9	0.0	0.0
201947	2	2	129.3	0.0	0.3	13.3	0.0	0.0
201947	2	3	97.7	0.0	0.4	13.5	0.0	0.0
201949	1	1	365.7	0.0	0.0	20.2	0.0	0.0
201949	1	2	312.6	1.5	80.7	28.7	0.0	200.8
201949	1	3	331.2	0.0	0.0	28.4	0.0	0.0
201949	2	1	69.5	0.0	0.0	30.0	0.0	0.0
201949	2	2	68.6	0.0	0.0	29.9	0.0	0.0
201949	2	3	67.0	0.0	0.0	25.2	0.0	0.0
201949	3	1	86.5	1.4	0.0	27.7	0.0	0.0
201949	3	2	96.7	1.4	0.0	21.9	0.0	0.0
201949	3	3	75.3	1.2	0.0	39.3	0.0	0.0
201949	4	1	127.2	5.0	0.0	10.3	0.0	0.0
201949	4	2	116.8	4.3	0.0	11.7	0.0	0.0
201949	4	3	138.1	5.2	0.0	10.9	0.0	0.0
201949	5	1	104.1	0.0	0.0	16.4	0.0	0.0
201949	5	2	111.4	0.0	0.0	14.7	0.0	0.0
201949	5	3	144.2	0.0	0.0	13.4	0.0	0.0
201949	6	1	156.9	0.0	0.0	17.3	0.0	0.0
201949	6	2	92.5	0.0	0.0	15.7	0.0	0.0
201949	6	3	127.8	0.0	0.0	11.6	0.0	0.0
201950	1	1	92.2	0.0	0.0	98.0	0.0	0.0
201950	1	2	70.5	0.0	0.0	118.9	0.0	0.0
201950	1	3	65.4	0.0	0.0	111.1	0.0	0.0
201954	1	1	126.4	0.0	0.0	23.8	0.0	0.0
201954	1	2	117.2	0.0	0.0	24.5	5.2	0.0
201954	1	3	87.6	0.0	0.0	19.4	0.0	0.0
201955	1	1	135.8	0.0	0.0	44.6	0.0	0.0
201955	1	2	127.0	0.0	0.0	42.1	0.0	0.0

Table 2. continued

GSWA sample no.	Nugget no.	Traverse line	Cu	Sb	Te	Hg	Pb	Bi
201955	1	3	136.4	0.0	0.0	75.2	0.0	0.0
201955	2	1	74.5	0.0	0.0	54.5	0.0	0.0
201955	2	2	70.8	0.0	0.0	55.0	0.0	0.0
201955	2	3	67.5	0.0	0.0	58.1	0.0	0.0
201955	3	1	113.1	0.0	0.0	60.2	0.0	0.0
201955	3	2	106.2	0.0	0.0	63.5	0.0	0.0
201955	3	3	97.2	0.0	0.0	67.0	0.0	0.0
201955	4	1	117.5	0.0	0.0	68.0	0.0	0.0
201955	4	2	126.2	0.0	0.0	70.9	0.0	0.0
201955	4	3	124.2	0.0	0.0	65.4	0.0	0.0
201956	1	1	120.7	0.0	0.0	49.7	0.0	0.0
201956	1	2	146.4	0.0	0.0	45.5	0.0	0.0
201956	1	3	114.3	0.0	0.0	49.5	0.0	0.0
201956	2	1	31.3	0.0	0.0	101.0	0.0	0.0
201956	2	2	42.1	0.0	0.0	77.8	0.0	0.0
201956	2	3	41.5	0.0	0.0	71.2	0.0	0.0
201957	1	1	57.8	0.0	0.0	67.5	0.0	0.0
201957	1	2	51.5	0.0	0.0	62.8	0.0	0.0
201957	1	3	67.7	0.0	0.0	88.7	0.0	0.0
201958	1	1	82.7	0.0	0.0	35.6	0.0	0.0
201958	1	2	83.0	0.0	0.0	41.2	0.0	0.0
201958	1	3	82.5	0.0	0.0	28.6	0.0	0.0
201960	1	1	40.6	0.0	0.0	55.5	0.0	0.0
201960	1	2	36.9	0.0	0.0	47.3	0.0	0.0
201960	1	3	47.4	0.0	0.0	48.6	0.0	0.0
201960	2	1	86.5	1.4	0.0	27.7	0.0	0.0
201960	2	2	137.3	0.0	0.0	59.8	0.0	0.0
201960	2	3	139.6	0.0	0.0	73.2	0.0	0.0
201960	3	1	76.1	1.3	0.0	46.6	0.0	0.0
201960	3	2	71.8	1.5	0.0	40.7	0.0	0.0
201960	3	3	66.8	1.9	0.0	38.8	0.0	0.0
201962	1	1	142.8	0.0	0.0	8.7	0.0	0.0
201962	1	2	147.7	0.0	0.0	11.3	0.0	0.0
201962	1	3	140.5	0.0	0.0	9.4	0.0	0.0
201962	2	1	54.6	0.0	0.0	21.0	0.0	0.0
201962	2	2	59.0	0.0	0.0	23.0	0.0	0.0
201962	2	3	56.6	0.0	0.0	25.5	0.0	0.0
201964	1	1	111.2	0.0	0.0	22.4	0.0	0.0
201964	1	2	115.9	0.0	0.0	22.9	0.0	0.0
201964	1	3	116.5	0.0	0.0	22.5	0.0	0.0
201964	2	1	13.7	0.0	0.0	29.6	0.0	0.0
201964	2	2	12.5	0.0	0.0	38.3	0.0	0.0
201964	2	3	13.4	0.0	0.0	33.6	0.0	0.0

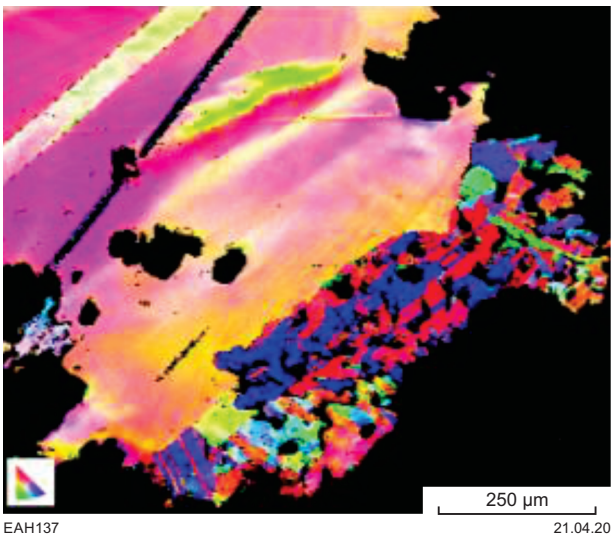

Figure 8. Electron back-scattered diffraction (EBSD) image of polished gold surface showing intensive twinning and polygranular dissolution structure of initially formed corrosive zone, GSWA 201962

Nuggets from the Camp Gully, Minters Gully and Hakes Patch areas contain mineral inclusions typical of those present in gold from bedrock mineralization. For example, galena inclusions with a Cu–Pb–Bi mineral phase were only identified in the Camp Gully area. Whereas, Ag–Pb tellurides are present in gold grains from the Minters Gully and Hakes Patch areas. Calcite crystals and other carbonates with Al clays, quartz and fine secondary gold particles fill fissures, cavities and voids in nuggets from the Six Mile, Camp Gully, and Minters Gully areas.

The spongy-textured gold nugget from the Six Mile area is unique in that it hosts inclusions of arsenopyrite and pyrite. The As content of the gold is elevated relative to the other gold nuggets in the collection. In addition, the gold has elevated copper and lower concentrations of Ag content (3 wt%). These compositional differences suggest that this nugget may have a different primary mineralization source compared with other nuggets identified in the Kurnalpi goldfield.

Gold nuggets derived from proximal areas to primary sources show some evidence for recrystallization, including the incipient recrystallization of rims related to erosion processes. Partial recrystallization of gold nuggets around regolith-derived mineral inclusions results from plastic deformation and chemical leaching of Ag in the weathering environment. Also during bushfires, when surface temperatures reach 850ºC, gold grains most likely partially melted and annealed, capturing surrounding gangue minerals.

Simple and polysynthetic coherent and incoherent twins were observed in some nuggets (Fig. 7b). They form by mechanical deformations during gold precipitation and by post-depositional dislocations.

The zoning shown in sample GSWA 201944 (Fig. 7c) is interpreted to be a result of acid (CrO_3 in HCl) etching where a fine film has formed on the surface of gold from the 'Beilby layer' (Hough et al., 2007). The film is translucent, highlights polishing artefacts and appears not to be influenced by crystallographic orientations. However, the film is sufficiently crystalline to define a polysynthetic twinning pattern on the surface of the sample, which in part reflects optically visible, well-defined lattice planes (Fig. 9). The unclear zoning appears to be a fabric of mildly deformed, but not annealed, gold crystals (Butt and Timms, 2011). Oscillatory zoning is a well-known microstructural characteristic of low-temperature epithermal gold formed from supersaturated solutions with more than 10% Ag (Petrovskaya, 1974; Nikolaeva et al., 2004; Butt and Timms, 2011). Nikolaeva et al. (2004) described unclear zoning microstructure patterns in deformed placer gold from a number of locations in Russia and indicated their rapid growth nature. Oscillatory zoning is common for many other minerals grown in nature from supersaturated fluids. This process reflects the coupling between the diffusion coefficient and the growth rate on the surface-reaction interface that leads to periodic instabilities in chemical composition without involvement of externally controlled parameters (Prieto et al., 1993).

In summary, gold nuggets from areas proximal to their inferred primary source are characterized by:

- a slightly transformed rounded morphology due to their short travel distances or/and prolonged residence in regolith
- two types of supergene recovery environments: Fe and Ca rich
- fine-grained inclusions of arsenopyrite, pyrite, galena, and Ag and Pb tellurides
- two distinctive concentrations of Ag: 3–5% and 9–12%
- low to slightly elevated Cu (30–300 ppm) and low Hg (10–100 ppm) contents; trace contents of Sb and Pb
- minor local recrystallization by mechanical deformation and unclear zoning microstructures with some twin planes and weakly developed recrystallized rims.

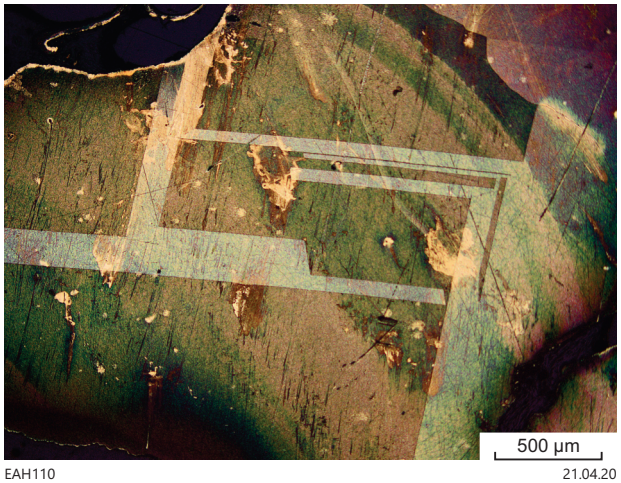

Figure 9. Reflected light photomicrographs of cut, polished and acid (CrO_3 in HCl) etched gold nugget showing translucent, sufficiently crystalline film formed from the 'Beilby layer' on the surface of gold sample GSWA 201944 (refer to text for explanations)

Table 3. ICP-MS vs LA-ICP-MS data of Ag and trace elements in gold sample GSWA 201944, in counts per second

Sample no.	*Method*	*Na23*	*Mg25*	*Al27*	*K39*	*Ti49*	*V51*	*Mn55*	*Co59*	*Ni60*	*Cu65*	*Zn66*	*As75*	*Se77*
201944-1	ICP-MS	20345	357	3845	20533	11	16	15	19	52	57791	184	213	0
201944-2	ICP-MS	0	158	1563	9579	12	0	16	0	28	57031	88	92	0
201944-3	ICP-MS	0	513	3487	15478	26	13	155	14	45	51282	96	127	0
201944-1	LA-ICP-MS	0	0	79	0	0	0	0	0	0	17946	0	0	59
201944-2	LA-ICP-MS	0	0	0	0	0	0	0	0	0	24017	0	0	0
201944-3	LA-ICP-MS	0	0	0	0	0	0	0	0	0	25813	0	0	0

Sample no.	*Method*	*Rb85*	*Sr88*	*Zr90*	*Pd108*	*Ag109*	*Cd111*	*Sn120*	*Sb121*	*Te126*	*Ba 138*	*Hg202*	*Tl205*	*Pb208*	*Bi209*
201944-1	ICP-MS	43	56	24	23	59332016	10	520	114	54	76	34786	12	73	70
201944-2	ICP-MS	0	16	17	15	43832417	0	343	324	28	33	20130	0	49	0
201944-3	ICP-MS	12	44	31	20	60767572	0	304	239	45	56	25200	17	40	35
201944-1	LA-ICP-MS	0	0	0	0	16963233	0	10	62	17	0	7301	0	0	0
201944-2	LA-ICP-MS	0	0	0	0	17545352	0	13	259	14	0	5831	0	0	0
201944-3	LA-ICP-MS	0	0	0	0	18232507	0	14	220	16	0	6115	0	0	0

Characterization of gold nuggets from areas distal to primary sources

Roundness of gold nuggets increases with greater distances of transportation, or longer burial times. Rounded nuggets display a higher frequency of mechanical and chemical transformations, fewer quartz and other hypogene mineral inclusions, a depletion in Ag content, and the development of a pronounced rim, defined by recrystallization and translation zones between residual areas and recrystallized parts of the nuggets (Nikolaeva et al., 2004).

The gold nugget from the Spud Flat area (Table 4) is the most mechanically deformed sample from the GSWA collection (Fig. 4a). Initially reniform, it has been rounded and flattened to a plate geometry before being folded and capturing ilmenite and mixed clay inclusions. However, its microstructure shows only very localized recrystallization along rims and around mineral inclusions, but no polycrystalline annealing fabrics. Instead, there are simple coherent twin planes and large, well-developed intergranular veinlets. The nuggets contain 30–200 μm-diameter partly dissolved Ag–Te-rich mineral inclusions, and elevated contents of Pb (up to 28 ppm), which potentially indicate nano-inclusions of galena. The nugget preserves some of the original microstructures and mineral inclusions despite the high degree of mechanical deformation and leaching of Ag in the supergene environment.

A well-rounded nugget from the Red Kettle area shows well-defined microstructures, such as a <500 μm-wide, recrystallized marginal rim and granoblasts with high-purity intergranular gold veinlets (Fig. 7f). Intensive development of intergranular gold veinlets can result from initial hypogene deformation and grain recrystallization, with continued Ag and other trace elements leaching and disintegration of spaces along intergranular veinlets in the supergene environment (Nikolaeva et al., 2004), where they were filled with clay and fine-grained secondary gold. The nugget contains 10–12 wt% Ag, the highest in the area, and is free from micro-inclusions or detectable trace elements. Thus, in comparison with other specimens, this gold nugget possibly presents a different type of primary mineralization, but was deposited in a distal area to the primary location.

Two other well-rounded gold nuggets from the Red Kettle and Sparkle sites also display exceptional trace-element characteristics. Both nuggets contain Bi and Te concentrations up to 200 and 100 ppm, respectively. By contrast, Ag, Cu and Hg display abundance levels that are comparable across the study area. Several micro-inclusions of bismuth telluride and telluric bismuth (tetradymite) were detected in the Sparkle sample, presumably reflecting the elevated contents of Bi and Te detected in the nugget.

Most nuggets in the gold collection are medium to well rounded. They have travelled intermediate distances from their primary sources, or they have experienced in situ alteration during their prolonged weathering. Apart from displaying a rounded shape, coating by regolith minerals, and well-developed intergranular veinlets filled with fine-grained gold, most of these nuggets possess characteristics similar to the less-rounded (i.e. proximal) specimens, including:

- Fe- and Ca-rich coatings and rounded maghemite inclusions
- small, rounded inclusions of galena, chalcopyrite, and partly leached Ag, Pb, and Bi telluride inclusions
- silver contents of 5–12 wt%
- Cu and Hg are consistently detected, with rare low abundances of Sb, Te, Bi, Pb, Al, Fe, and Mg
- polycrystalline microstructure for gold aggregates; local recrystallization around regolith inclusions; some margins formed by mechanical deformation and chemically leached of Ag; twin planes
- some original zonation in the formation of their microstructures
- only thin (<200 μm) recrystallized rims.

These characteristics are typical for locally derived gold nuggets that have not been transported far from their primary source areas, but have been significantly altered by in situ weathering.

Likely sources for the analysed gold nuggets in the Kurnalpi goldfield

Several styles of primary gold mineralization are identified in the Kurnalpi goldfield based on the mineralogical characteristics of the collected gold nuggets, including their mineral inclusions, chemistry and microstructures.

As discussed above, variations in gold mineralogy are limited to:

- intergrowths with milky quartz, large inclusions of maghemite
- coatings of Fe- and Ca-rich clays
- Ag content from 3 to 12 wt%
- micro-inclusions of calcite, galena, arsenopyrite, pyrite and numerous Ag(Au) tellurides
- traces of Cu and Hg, and rare Sb, Pb, Bi, Te, Al, Fe and Mg
- polycrystalline internal structure with twin planes, local recrystallization, and fine-grained rims.

Bedrock-hosted gold mineralization at the Scottish Lass and Brilliant prospects is mainly associated with quartz veins and quartz–pyrite±carbonate±hematite alteration in metabasalt, and magnetite-bearing granophyric quartz dolerite dykes that cut ultramafic rocks (Swager, 1994; Steuart, 2001; Gunther, 2004). The very limited transportation of studied gold nuggets suggests their local origin from these quartz veins, which are likely to be expressions of orogenic gold deposits documented in greenstone belts throughout the Yilgarn Craton (e.g. Groves et al., 1998). Most gold nuggets have low Ag and Cu contents, and host sulfide and telluride inclusions.

Table 4. Summary of gold characteristics

GSWA sample no.	No. of nuggets	Site	Shape	Micro-inclusions	Microstructure	Ag wt%	Cu ppm	Hg ppm	Other traces (ppm)
			Angular and slightly rounded gold nuggets (residual)						
201930	4	Six Mile	Intergrowth with milky quartz; clay-Fe oxide coatings	Calcite in fissures; arsenopyrite and pyrite; rounded and angular	Twinning simple and polysynthetic, local recrystallization	3–7	200–300	40–100	
201941 201942 201943	7	Camp Gully	Intergrowth with milky quartz, maghemite, ilmenite; clay–carbonate–Fe oxide coatings	Calcite in fissures; galena rounded with fine CuPbBi inclusion	Coherent twinning	7–11	100–200	10–40	
201947 201962	3	Minters Gully	Clay–Fe oxide coatings; free from quartz	Calcite in fissures; Ag(Au)Te rounded	Unclear zoning and fine rim in monocrystal	3–9	60–150	10–70	
201949	1	Sparkle	Intergrowth with maghemite			5	120	10	Sb(5)
201950 201951 201954	Over 50	Southwest from Discovery Hill	Intergrowth with milky quartz; clay–Fe oxide coatings			3–5	70–130	20–100	Pb(5)
201955 201956 201957	9	Hakes Patch	Intergrowth with brown quartz; brown and black coatings	PbTe (altaite), Ag(Au)Te rounded		4–6	30–140	50–100	Al(17) Fe(17) Mg(5)
			Well and perfectly rounded gold nuggets (altered)						
201946	1	Spud Flat	Flattened, rounded and then folded in half preserving mixed clays from regolith; surface smooth and pitted with ferruginous material, few grooves	Large Ag(Au)Te inclusions, partially leached; rounded ilmenite	Well-developed veinlets with pure gold; Ag-leached rim	7–8	180	6	Pb(28)
201949	6	Sparkle	White clay coating; smooth even surface, maghemite inclusion	Small BiTe inclusions, such as tetradimit, partially leached, rounded galena	Numerous well-developed veinlets with pure gold	4–7	100–330	15–25	Te(81) Bi(201) Sb(1.5)
201960	3	Lower Italian Gully	Flattened elongated plates with rugged and even surfaces, clean from inclusions and coatings	Lost during polishing					

Both characteristics are compatible for orogenic gold deposits, but are atypical for copper-rich porphyry, iron oxide–copper–gold (IOCG), high Cu and Bi gold-skarn, and epithermal Ag-rich deposits (Hancock, 2018). However, elevated Ag and Sb contents, and the presence of telluride micro-inclusions in some gold nuggets from the Six Mile, Camp Gully, and Sparkle areas, are compatible with low-sulfidation epithermal gold mineralization occurrences in the far east of Russia (Nikolaeva et al., 2004). Furthermore, the subset of gold nuggets with elevated Cu and Bi concentrations from the Six Mile, Red Kettle, Halfway Hill, Purple Patch and Sparkle areas are compatible with porphyry or gold-skarn mineral systems (Nikolaeva et al., 2004; Hancock, 2018). Alternatively, the Cu-rich phases observed in the recrystallized parts of gold grains can be indicative of their secondary origin.

The nuggets with exceptionally low Ag contents from Six Mile, Discovery Hill and Minters Gully are unlikely to be products of multi-reworking. Instead, they probably result from a low-silver mineralization event. Arsenopyrite and pyrite inclusions in one gold nugget from the Six Mile area suggest the presence of a never-before described, gold–arsenopyrite–pyrite mineralization event in the Kurnalpi goldfield. In general, the wide occurrence of telluride inclusions and unclear zoning in the studied gold nuggets are characteristics of gold deposits formed at shallow (<1 km) crustal levels (Nikolaeva et al., 2004).

One last speculation about the origin of gold nuggets relates to the single gold crystal (GSWA 201962) from Minters Gully (Fig. 10a). The surface of this gold was etched by IBM and was observed under low-pressure BSE. The images show pitted semispherical texture that clearly relates to the hardness/toughness of the sample's surface (Fig. 10b,c). The larger concavities suggest a softer surface, while smaller directional pits that are derived from mechanical scratches indicate a harder more compressed gold surface. Distal background areas contain nano-scale concavities that are not directional. According to Halfpenny et al. (2013), these types of concavities are most likely created by the IBM process. However, our study of the gold standard (AuRM2), which was created by blending and stirring of a pure gold melt (Murray, 2009), demonstrates that this standard has smooth texture without concavities, even after prolonged IBM (Fig. 10d). Therefore, we believe that the concaved micro-texture observed in GSWA 201962 is a consequence of the nanoparticulate fabric of native gold. Pearce et al. (2016) and Burke et al. (2017) provide direct evidence of nanoparticulate composition of gold and describe its deposition from colloidal suspensions.

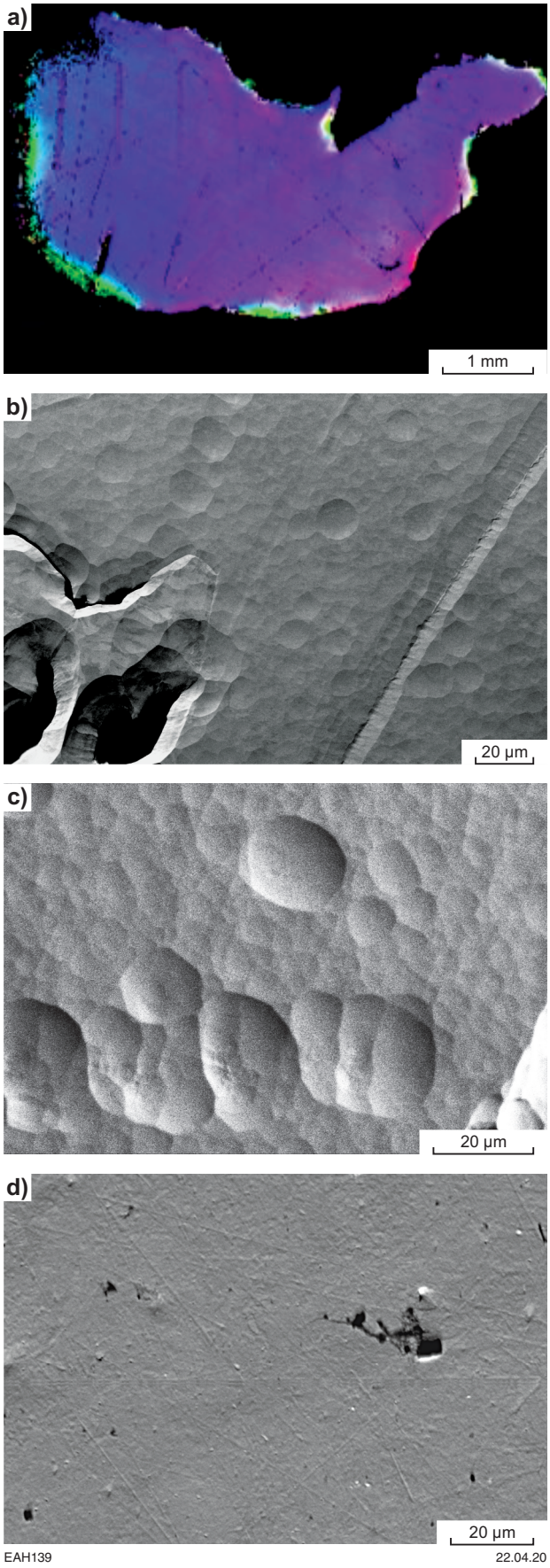

Figure 10. Ion Beam Milling (IBM) method of polishing gold surface: a) EBSD image of cut gold crystal, polished with diamond paste prior to IBM, and showing only one crystallographic plane, GSWA 201962; b) SEM image of the same sample after polishing with IBM for over 12 hours; c) benchtop SEM enlarged image of the same sample; d) SEM image of AuRM2 standard surface after polishing with diamond paste and then with IBM for over 12 hours. See explanation in text

Supergene alteration of gold nuggets

The ability to discriminate supergene from hypogene processes is critical for interpreting likely sources of primary gold mineralization. The gold nuggets in this study record different intensities of supergene alteration caused by their prolonged burial in the regolith. Supergene processes affect gold nugget morphology, inclusions, microstructure and chemistry.

For instance, the high Cu (< 600 ppm) and Hg (< 4000 ppm) phases in partly recrystallized gold nuggets from the Six Mile and Halfway Hill areas are interpreted to be the products of interaction between Cu- and Hg-rich fluids with gold nuggets during their residence in the regolith. During that time, selective dissolution-(re)precipitation and subsequent recrystallization took place in deformed zones around maghemite and goethite inclusions, as well as along rims and voids that are interconnected to the exterior of the nugget. These processes resulted in the leaching of Ag and increases in the Cu and Hg content of the nuggets.

Marginal rims

The studied gold nuggets were altered in situ or during only short transportation distances away from their primary source. Consequently, their mineral inclusions are commonly preserved and the nuggets develop only thin marginal rims.

Several gold nuggets display porous dissolution zones along their margins that are easily detected in reflected light. EBSD analysis of one of these zones revealed the existence of intensive twinning and polygranular dissolution structures that are related to corrosion along the nugget margin (Fig. 8). In another sample, a compacted Ag-free corrosive rim, less than 20 µm width, overgrows the recrystallized margin (Fig. 11).

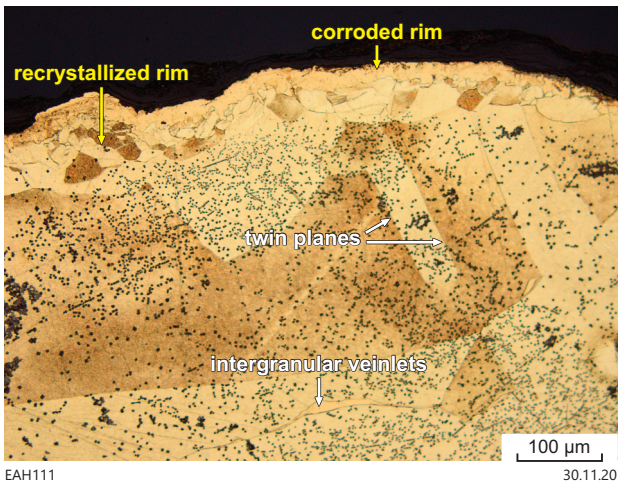

Figure 11. Reflected light photomicrographs of cut, polished and aqua regia etched well-rounded gold nugget showing thin corroded rim of pure gold mantling thicker recrystallized marginal rim, twin planes and intergranular veinlets (there are dark spots of AgCl crystals), GSWA 201933

Two different processes, and commonly their combination, are involved in the formation of high-purity corrosive rims and recrystallized rims: i) intensive deformations and dislocations along the margins of gold grains lead to the annealing of damage structures and growth of undeformed crystals (Petrovskaya, 1973; Hough et al., 2009), or strain-driven solid state recrystallization with Ag expulsion (Stewart et al., 2017). This type of recrystallization can be referred to as the 'dry' process; ii) in the more common dissolution-(re)precipitation case, when solutions are involved (i.e. the 'wet' process), the relatively soluble Ag is partly leached from gold grains exteriors with subsequent recrystallization of unstable Ag-depleted structures. Besides, electrochemical reaction between acidic fluid and Au–Ag binary solid alloys lead to dissolution of Ag and formation of corrosive rim with pure gold (Nikolaeva et al., 2004).

In some cases, the corrosive rim can resemble the aggregations of secondary gold, formed by (re)precipitation of dissolved gold particles on the surface of detrital gold grains or by microbiological activity. The corrosive rim forms in situ with sharp recrystallized contact with the parental grain (Fig. 8). The secondary gold is commonly fragile, spongy and precipitates on limited exterior surfaces and preserves in cavities and voids (Fig. 7h). Stewart et al. (2017) interpreted the presence of delicate gold overgrowths on surfaces of recrystallized Otago alluvial gold 'as a result of combination of dissolution and reprecipitation of gold by groundwater', that, by our interpretation, is the most likely evidence of secondary gold rather than a partial corrosive rim.

Intergranular veinlets

Many well-rounded gold nuggets show well-developed intergranular veinlets filled with fine-grained gold, clays and other regolith material. Their origin is the same dissolution processes described for the formation of marginal rims, but is not restricted to supergene alteration. Hypogenic transformations associated with hydrothermal activities can be involved in the initial formation of the intergranular veinlets in a crystal aggregate (e.g. Bangemall Mining Centre, Hancock et al., 2009; Glenburgh, Roche, 2016) and even lead to disintegration of gold grains. In regolith environments, inorganic chemical reactions promote Ag leaching along intergranular/crystal boundaries; thickening and recrystallizing these boundaries and form 'cracks' or 'channels' that are filled with regolith minerals (Figs 7h, 12). Intergranular veinlets are more protected from the surrounding environment than exterior rims and have a greater opportunity for development. They have not been reported in young placer gold (Nikolaeva et al., 2004) and, therefore, can be diagnostic for prolonged burial alteration processes.

Conclusions and further work

The 75 selective gold nuggets in this study are small to medium sized with a weight range from 0.3 to 18.8 g. These samples were sourced from 36 sites over an area of about 80 km^2 in the Kurnalpi goldfield. All nuggets have an interpreted hypogene origin, based on their high Ag content, mineral inclusions, and crystalline microstructure.

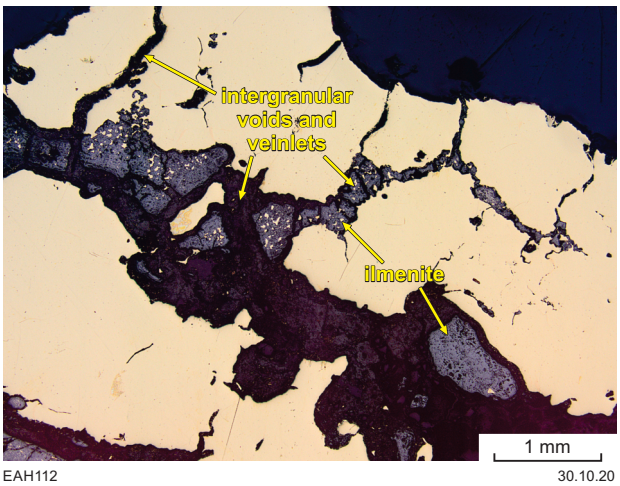

Figure 12. Reflected light photomicrographs of cut and polished gold nugget showing well-developed, thick intergranular voids and veinlets filled with ilmenite, Fe oxides, ferruginous clay and fine gold particles, GSWA 201960

They were transported short distances from their primary gold mineralization sources and were affected by in situ alteration processes during their prolonged residence in the regolith. About 30% of the collected gold nuggets have characteristics of bedrock-hosted gold, with limited alteration during residence time. Original microstructures are commonly preserved and not significantly changed by any regional hydrothermal or metamorphic events. The nuggets record only local recrystallization around areas of incorporated regolith mineral inclusions and along thin marginal rims that formed by supergene recovery deformation and alteration. Variations in gold morphology and regolith inclusions are characteristic of their local supergene environments during gold deposition and residence time.

The primary source for the gold nuggets is compatible with examples of known quartz vein-related gold deposits in the Kurnalpi goldfield, with two types of mineral assemblages identified: a gold–arsenopyrite–pyrite and a gold–galena–chalcopyrite, and Te- and Bi-bearing minerals assemblage. Although nuggetty gold mineralization is unknown at local deposits, mineralization styles and depth of crustal formation are broadly compatible. This suggests the Kurnalpi goldfield remains prospective for the discovery of both these styles of orogenic gold deposits, targeting locations Camp Gully, Minters Gully, Discovery Hill, Hakes Patch, Six Mile and Sparkle. These sites have accumulated gold eroded from local basement deposit(s) either by exposure to different vertical levels of mineralization, by lateritic erosion of several local primary sources within the area, or by a combination, and therefore can be prospective for further exploration.

Detailed study of gangue minerals in the gold nuggets, such as maghemite, ilmenite, carbonates and ferruginous clays may provide more information about the transport and alteration history of gold nuggets and their affiliation with bedrocks in the area.

Acknowledgements

The authors gratefully acknowledge Wade Johnson and Lijun Yang from KalNorth Gold Mines Limited for the donation of gold nuggets and especially Wade Johnson for his initiation, support and ongoing contributions to this project. We thank Michael Verrall for his help with the SEM-EDX, EBSD, and IBM instruments and Derek Winchester for the preparation of gold sections at CSIRO, Kensington, Western Australia.

We are particularly grateful to John Watling and Chris May from TSW Analytical for providing LA-ICP-MS data.

References

Anand, RR and Butt, CRM 2010, A guide for mineral exploration through the regolith in the Yilgarn Craton, Western Australia: Australian Journal of Earth Sciences, v. 57, p. 1015–1114.

Beardsmore, TJ and Gardner, Y 2003, Darlot gold deposit, Yandal gold province, Yilgarn Craton, Western Australia, *in* CSIRO Explores 1: Yandal Gold Province: Geoscience and Exploration Success *edited by* KS Ely and GN Phillips: CSIRO Exploration and Mining, Melbourne, p. 173–219.

Burke, M, Rakovan, J and Krekeler, MPS 2017, A study by electron microscopy of gold and associated minerals from Round Mountain, Nevada: Ore Geology Reviews, v. 91, p. 708–717.

Butt, CRM and Timms, NE 2011, The Liversidge nugget collection: A new look at some old gold: Australian Journal of Earth Sciences, v. 58, p. 777–791.

Chapman, RJ, Leake, RC and Styles, MT 2002, Microchemical characterisation of alluvial gold grains as an exploration tool: Gold Bulletin, v. 35, no. 2, p. 53–65.

Eyles, N and Broekert, P de 2001, Glacial tunnel valleys in the Eastern Goldfields of Western Australia cut below the late Paleozoic Pilbara ice sheet: Palaeogeography, Palaeoclimatology, Palaeoecology, v. 171, p. 29–40.

Groves, DI, Goldfarb, RJ, Gebre-Mariam, M, Hagemann, SG and Robert, F 1998, Orogenic gold deposits: A proposed classification in the context of their crustal distribution and relationship to other gold deposit types: Ore Geology Reviews, v. 13, no. 1–5, p. 7–27.

Gunther, L 2004, Kurnalpi Joint Venture: annual report for the period 12 January 2003 to 31 December 2003: Newcrest Mining Limited: Geological Survey of Western Australia, Statutory mineral exploration report A68099, viewed 13 February 2019, 12p.

Halfpenny, A, Hough, RM and Verrall, M 2013, Preparation of samples with both hard and soft phases for electron backscatter diffraction: examples from gold mineralization: Microscopy and Microanalysis, Microscopy Society of America, p. 1–12.

Hancock, EA, Thorne, AM, Morris, PA, Watling, RJ and Cutten, HNC 2009, Mineralogy and trace element chemistry of lode and alluvial gold from the western Capricorn Orogen: Geological Survey of Western Australia, Record 2009/6, 29p.

Hancock, EA and Thorne, AM 2011, Mineralogy of lode and alluvial gold from the western Capricorn Orogen, Western Australia: Australian Journal of Earth Sciences, v. 58, p. 793–801.

Hancock, EA, Watling, RJ and Beardsmore, TJ 2017, Quantitative trace-element analysis of gold using LA-ICP-MS and implications for the mechanism of native gold crystallization, *in* Abstracts: 2017 TIGeR Conference: Timescales of Geological Processes, Perth, Western Australia, 13–15 September 2017: Curtin University, p. 51.

Hancock, EA 2018, Applying gold fingerprinting to mineral prospectivity studies, *in* Abstracts, Gold18@Perth, Western Australia, 2–3 August 2018: Australian Institute of Geoscientists, p. 28–30.

Hough, RM, Butt, CRM, Reddy, SM and Verrall, M 2007, Gold nuggets: Supergene or hypogene? Australian Journal of Earth Sciences, v. 54, p. 959–964.

Johnson, WS 2014, Combined annual report for the period ending 13 April 2014, C101/2011 Kurnalpi project: KalNorth Gold Mines Limited: Geological Survey of Western Australia, Statutory mineral exploration report A103481, 8p.

Jutson, JT 1914, Kurnalpi, north-east Coolgardie Goldfield, *in* Miscellaneous reports, Series III, Nos. 33-51: Geological Survey of Western Australia; Bulletin, p. 13–30.

Liversidge, A 1893, On the origin of gold nuggets: Journal and Proceedings of the Royal Society of New South Wales, v. 27, p. 303–343.

Martin, DMcB, Johnson, SP and Riganti, A 2016, 1:500 000 State interpreted bedrock geology of Western Australia, 2016: Geological Survey of Western Australia, digital data layer, <www.dmirs.wa.gov.au/geoview>.

Montgomery, A 1905, Report on the state of mining progress in the Kurnalpi, Mulgabbie, Pinjin, Edjudina, Yarri and Yerilla districts, Department of Mines annual report.

Murray, S 2009, LBMA certified reference materials. Gold project final update: The London Bullion Market Association, Alchemist, no. Fifty-five, p. 11–12.

Nikiforova, ZS, Gerasimov, BB and Tulaeva, EG 2011, Genesis of gold-bearing placers and their possible sources (Eastern Siberian Platform): Lithology and Mineral Resources, v. 46, no. 1, p. 17–29.

Nikiforova, ZS, Gerasimov, BB, Glushkova, EG and Kazhenkina, AG 2013, Gold resource potential of the eastern Siberian Platform: Geology of Ore Deposits, v. 55, no. 4, p. 265–277.

Nikolaeva, LA, Gavrilov, AM, Nekrasova, AN, Yablokova, SV and Shatilova, LV 2004, Native gold in lode and placer deposits of Russia, Atlas: Central Research Institute of Geological Prospecting for Base and Precious Metals (TsNIGRI), Moscow, Atlas, 176p.

Nikolaeva, LA, Nekrasova, AN, Milyaev, SA, Yablokova, SV and Gavrilov, AM 2013, Geochemistry of native gold from deposits of various types: Geology of Ore Deposits, v. 55, no. 3, p. 176–184.

Pearce, MA, Gazley, MF, Fisher, LA, Hough, RM, Saunders, M and Kong, C 2016, Nanoparticles and gold deposit formation, *in* Goldschmidt Conference Abstracts, Goldschmidt Conference, Yokohama, Japan, 26 June – 1 July 2016, p. 2455.

Petrovskaya, NV 1973, Native gold: Nauka, Moscow, Russia, 347p.

Prieto, M, Putnis, A and Fernández-Díaz, L 1993, Crystallization of solid solutions from aqueous solutions in a porous medium: zoning in $(Ba,Sr)SO_4$, v. 130, no. 3, p. 289–299.

Roche, LK 2016, Unravelling the upper-amphibolite facies Glenburgh gold deposit, Gascoyne Province — evidence for metamorphosed mineralization: Geological Survey of Western Australia, Report 155, 44p.

Schupp, J 1985a, Kurnalpi Project — preliminary geological report: Metana Minerals NL: Geological Survey of Western Australia, Statutory mineral exploration report A15630, 12p.

Schupp, J 1985b, Kurnalpi Project — geological review: Metana Minerals NL: Geological Survey of Western Australia, Statutory mineral exploration report A17315, 26p.

Schupp, J 1985c, Kurnalpi Project — report on the results of the alluvial gold bulk sampling programme for Coronet Resources NL: Metana Minerals NL: Geological Survey of Western Australia, Statutory mineral exploration report A17305, 11p.

Schupp, J 1985d, Kurnalpi Project — report on the results of the alluvial gold bulk sampling programme for Teamwork Minerals PL: Metana Minerals NL: Geological Survey of Western Australia, Statutory mineral exploration report A17311, 19p.

Schupp, J 1985e, Kurnalpi Project — report on the results of the alluvial gold bulk sampling programme for Coopers Resources NL: Metana Minerals NL: Geological Survey of Western Australia, Statutory mineral exploration report A17314, 15p.

Schupp, J 1986a, Kurnalpi Project — alluvial gold sample test run results on Mining Lease M28/17 for Coronet Resources NL: Metana Minerals NL: Geological Survey of Western Australia, Statutory mineral exploration report A17316, 5p.

Schupp, J 1986b, Kurnalpi Project — alluvial gold sample test run results on Mining Lease M28/18 for Coopers Resources NL: Metana Minerals NL: Geological Survey of Western Australia, Statutory mineral exploration report A17317, 5p.

Steuart, P 2001, Kurnalpi annual report for the period 1 January to 31 December 2000: AngloGold Australasia Limited: Geological Survey of Western Australia, Statutory mineral exploration report A61986, 107p.

Stewart, J, Kerr, G, Halfpenny, A, Pearce, MA, Hough, RM and Craw, D 2017, Low temperature recrystallization of alluvial gold in paleoplacer deposits: Ore Geology Reviews, v. 88, p. 43–56.

Swager, CP 1994, Geology of the Kurnalpi 1:100 000 sheet: Geological Survey of Western Australia, 1:100 000 Geological Series Explanatory Notes, 19p.

Tetland, M 2015, Trace element analysis of placer gold: The University of British Columbia, Okanagan, Master of Science thesis, 206p.

Watling, RJ, Herbert, HK, Delev, D and Abell, ID 1994, Gold fingerprinting by laser ablation inductively-coupled plasma mass spectrometry: Spectrochimica Acta, 49B, no. 2, p. 205–219.

Wilson, AF 1984, Origin of quartz-free gold nuggets and supergene gold found in laterites and soils — a review and some new observations: Australian Journal of Earth Sciences, v. 31, no. 3, p. 303–316.

Hancock and Beardsmore

PROVENANCE FINGERPRINTING OF GOLD FROM THE KURNALPI GOLDFIELD

This Report evaluates the morphology, chemistry, microstructure and accessory inclusions of 75 small placer gold nuggets from the Kurnalpi Terrane, Western Australia, to determine the nature and origin of the bedrock source.

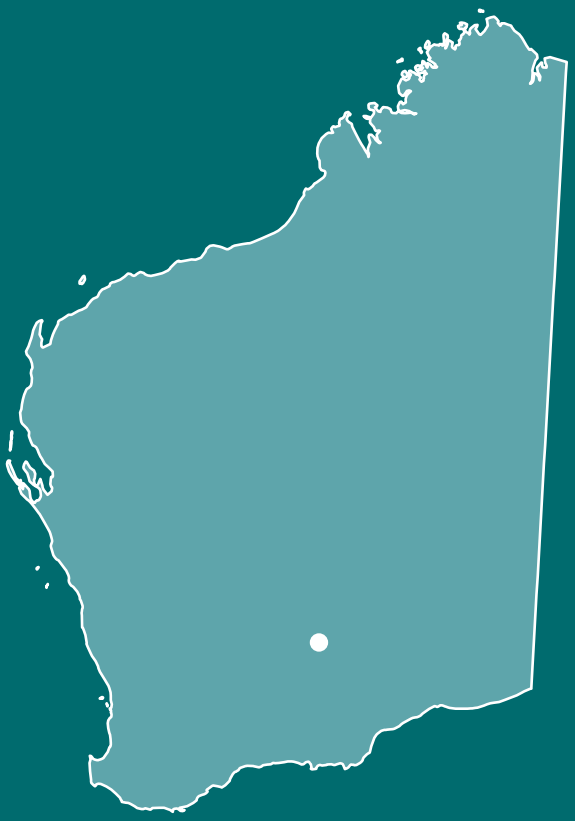

The nuggets discovered in buried paleochannels, Cenozoic laterite and calcrete deposits have a hypogene origin, and about 30% of them show bedrock-type characteristics, such as angular shape, intergrowth with milky quartz, mono- and polycrystalline microstructure, elevated (up to 12%) silver content and micro-inclusions of sulfides and tellurides. Other gold nuggets show rounded shape and well-developed intergranular veinlets filled with regolith material and fine-grained gold. However, their micro-inclusions, silver and trace element contents, and weakly developed recrystallized rims are typical for locally derived gold nuggets that have not been transported far from their primary source area. However, they have a long history of burial alteration in the regolith.

Nuggets were eroded from primary deposits of the greenstone-hosted quartz veins with possibly two mineralogical assemblages: gold–arsenopyrite–pyrite and gold–galena–chalcopyrite–tellurides.

Further details of geoscience products are available from:

Information Centre
Department of Mines, Industry Regulation and Safety
100 Plain Street
EAST PERTH WA 6004
Phone: (08) 9222 3459 Email: publications@dmirs.wa.gov.au

www.dmirs.wa.gov.au/GSWApublications

REPORT 212